Supporting Information

Polyoxometalate-based metal-organic supramolecular architectures derived from two new pyrimidine-amide ligands as supercapacitors and multifunctional electrochemical sensors

Xiu-Li Wang*[1], Jun-Jun Lu[1], Hong-Yan Lin, Qian-Qian Liu and Ke-Ke Chen

College of Chemistry and Materials Engineering, Bohai University, Professional Technology Innovation Center of Liaoning Province for Conversion Materials of Solar Cell, Jinzhou 121013, P. R. China.

X-ray Crystallographic Study

The single-crystal X-ray diffraction data for complexes **1**–**2** were collected using a Bruker SMART APEX II with Mo Kα radiation (λ = 0.71073 Å) by ω and θ scan mode at room temperature. Both structures were solved by direct methods with the Olex2 software.[1] The final refinement was performed by full matrix least-squares techniques on F^2. All non-hydrogen atoms were refined with anisotropic temperature parameters. All hydrogen atoms were placed in geometrically idealized position as a riding mode. The command "ISOR" was used to refine atoms C11 in complex **1** and C6 in complex **2**. The command "DFIX" was used to refine atoms H1Wa H2Wa in complex **1**. The command "DELU" was used to refine atoms N8 C13 C13 C8 C16 C8 C13 N8 C14 C15 Cu1 Cl1 N1 N9 O1 in complex **1**. The command "SADI" was used to refine atoms C16 C15 C8 C16 C8 C13 N8 C13 N8 C14 C15 C14 in complex **1**, and Co1 H2Wa Co1 H2Wb in complex **2**. The selected bond distances and angles for **1**–**2** are summarized in Table S1. The CCDC numbers are 2243305 and 2243304.

* Corresponding author. Tel: +86-416-3400160

E-mail address: wangxiuli@bhu.edu.cn (X.-L. Wang)

[1] These authors contributed equally.

Synthesis methods of pypa and bpap

Ligand pypa was synthesized as follows: 4-Pyrimidinecarboxylic acid (4g) and 50 mL of pyridine were added to a 250 mL distillation flask and stirred for 15 minutes. Then 3-(aminomethyl) pyridine (3.2 mL) was slowly added under stirring. And 10 mL of triphenyl phosphite was slowly added after stirring for 20 minutes. The mixture was refluxed for 10 hours. The product was cooled at room temperature and stood for two days, then filtered and rinsed with ethanol to obtain pale yellow crystalline solid.

The synthesis method of bpap is only to replace 3-(aminomethyl) pyridine with 1,5-pentanediamine (7.5 mL), the reflux time is changed to 8 hours, and other steps remain unchanged.

Preparation of complexes 1–2 modified carbon paper electrodes (1-cpe and 2-cpe)

The mixture of 5 mg complex **1** (or **2**) and 25 mg activated carbon was fully ground in a mortar. Then the above mixture was sonicated in a mixed solvent of water (300 μL) and ethanol (100 μL) for 1 hour to form a uniform turbid liquid. 100μL of well dispersed slurry was dropped onto the surface of the carbon paper (1 × 1 cm^2) and dried at 80℃ for 2 hours. Finally, 10 μL of Nafion solution was dropped onto the electrode surface, and the electrode was dried at room temperature. [2]

Preparation of complexes 1–2 bulk-modified carbon paste electrodes

The complexes **1**–**2** bulk-modified carbon paste electrodes (**1**-CPE and **2**-CPE) was fabricated by mixing 0.11 g graphite powder and 0.015 g complex **1** or **2** in an agate mortar for approximately 30 minutes to achieve a uniform mixture; then 0.10 mL paraffin oil was added and stirred with a glass rod. The homogenized mixture was packed into a 3 mm inner diameter glass tube and the tube surface was wiped with weighing paper. Electrical contact was established with a copper wire through the back of the electrode.

Electrochemical measurements

The specific gravimetric capacitance value can be calculated by Eq. (S1):

$$Cs = \frac{I\Delta t}{m\Delta V} \quad (\mathbf{1})$$

where Cs (F g^{-1}) represents the specific capacitance, I (A) represents the discharge current, ΔV (V) represents the potential change within the discharge time Δt (s), and m (g) corresponds to the amount of active material on the electrode.[3]

The energy density E (Wh kg^{-1}) and power density P (W kg^{-1}) of symmetrical supercapacitor can be calculated by Eq. (S2) and Eq. (S3):

$$E = \frac{1000 \cdot Cs \cdot \Delta U^2}{2 \cdot 3600} \quad (\mathbf{2})$$

$$P = \frac{3600 \cdot E}{\Delta t} \quad (\mathbf{3})$$

Where C, V, and Δt are the specific capacitance (F g^{-1}), operating voltage (V) and discharge time (s), respectively. [4]

The Eq. (S4) was used to calculate the limit of detection (LOD) of **1**-CPE and **2**-CPE to Cr(VI) and Fe(III):

$$LOD = \frac{S/N \cdot \sigma}{k} \quad (\mathbf{4})$$

S/N is the signal-to-noise ratio, and usually the value is 3. σ is the standard deviation, and k is the linear regression slope. [5]

Table. S1 Selected bond distances (Å) and angles (°) for complexes **1**–**2**.

Complex **1**			
Cu(1)-N(1)	2.004(3)	Cu(1)-N(9)	1.990(3)
Cu(1)-O(3)	2.625(3)	Cu(1)-O(1)	1.995(3)
Cu(1)-Cl(1)	2.2586(11)	Cu(1)-Cl(1)#1	2.7535(12)
Cl(1)-Cu(1)-Cl(1)#1	89.76(4)	Cl(1)-Cu(1)-O(3)	97.34(7)
O(1)-Cu(1)-Cl(1)#1	91.66(9)	O(1)-Cu(1)-Cl(1)	177.85(9)
O(1)-Cu(1)-O(3)	81.45(11)	O(1)-Cu(1)-N(1)	80.69(13)
O(3)-Cu(1)-Cl(1)#1	170.13(7)	N(9)-Cu(1)-Cl(1)	94.05(10)
N(9)-Cu(1)-Cl(1)#1	91.61(10)	N(9)-Cu(1)-O(1)	87.53(12)

N(9)-Cu(1)-O(3)	81.09(11)	N(9)-Cu(1)-N(1)	164.08(14)
N(1)-Cu(1)-Cl(1)#1	99.35(10)	N(1)-Cu(1)-Cl(1)	97.49(11)
N(1)-Cu(1)-O(3)	86.57(12)		
Symmetry code for **1**: #1 -x+1, -y+1, -z+1			
Complex **2**			
Co(1)-O(1)	2.098(7)	Co(1)-O(2)#2	2.126(7)
Co(1)-O(1W)	2.062(7)	Co(1)-O(2W)	2.024(8)
Co(1)-N(2)#2	2.143(9)	Co(1)-N(1)	2.133(9)
O(1)-Co(1)-O(2)#2	90.5(3)	O(1)-Co(1)-N(2)#2	95.7(3)
O(1)-Co(1)-N(1)	76.5(3)	O(2)#2-Co(1)-N(2)#2	76.4(3)
O(2)#2-Co(1)-N(1)	104.1(3)	O(1W)-Co(1)-O(1)	89.6(3)
O(1W)-Co(1)-O(2)#2	168.0(3)	O(1W)-Co(1)-N(2)#2	91.6(3)
O(1W)-Co(1)-N(1)	87.6(3)	O(2W)-Co(1)-O(1)	168.9(3)
O(2W)-Co(1)-O(2)#2	88.1(3)	O(2W)-Co(1)-O(1W)	94.1(3)
O(2W)-Co(1)-N(2)#2	94.7(3)	O(2W)-Co(1)-N(1)	93.2(3)
N(1)-Co(1)-N(2)#2	172.2(3)		
Symmetry code for **2**: #2 x-1, y, z			

Table S2. Selected hydrogen-bonding distance (Å) and angles (°) for complexes **1**–**2**.

Complex **1**				
D-H···A	D-H	H···A	D···A	D-H···A
N4-H4···O3W	0.86	2.00	2.781(7)	150
O2W-H2WB···N5	0.85	1.82	2.663(8)	172
O2W-H2WA···O1W	0.85	2.07	2.748(12)	136
O1W-H1WA···O3W	0.85	2.02	2.772(11)	148
Complex **2**				
D-H···A	D-H	H···A	D···A	D-H···A
N6-H6···O10	0.86	2.06	2.908(11)	167
N5-H5···O6	0.86	2.11	2.954(11)	169
O2W-H2WA···O3	0.85	2.04	2.683(11)	132

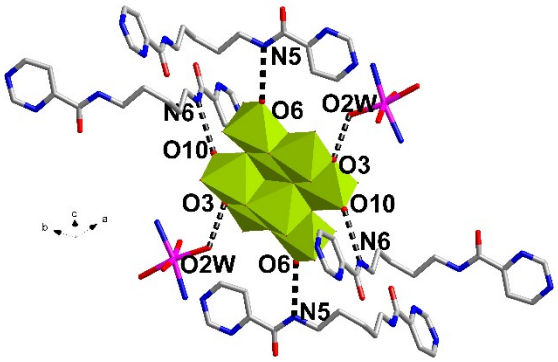

Fig. S1. The hydrogen bond diagram of Mo_8 anions in complex **2**.

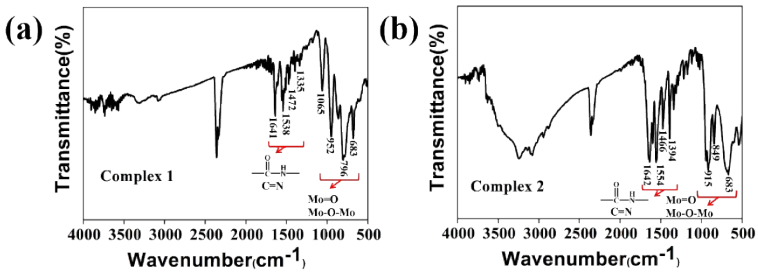

Fig. S2. (a-b) The IR spectra of complexes **1**–**2**.

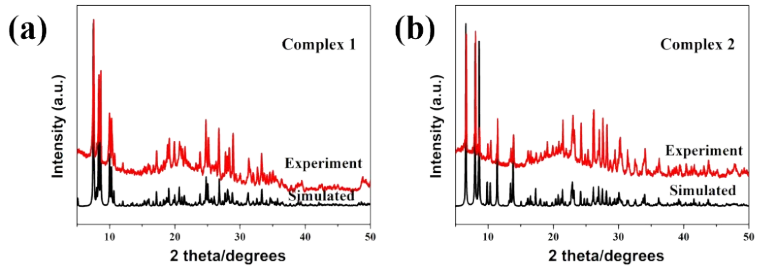

Fig. S3. (a-b) The PXRD patterns of complexes **1**–**2**.

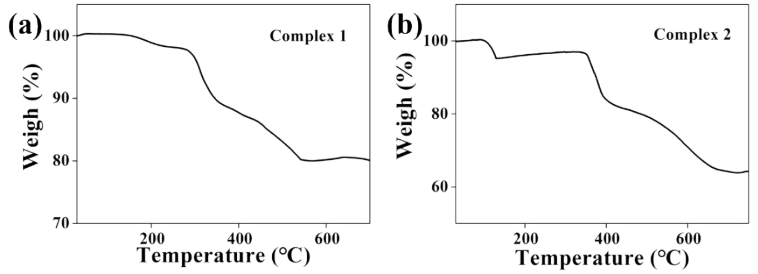

Fig. S4. (a-b) The TG curves of the complex **1**–**2**.

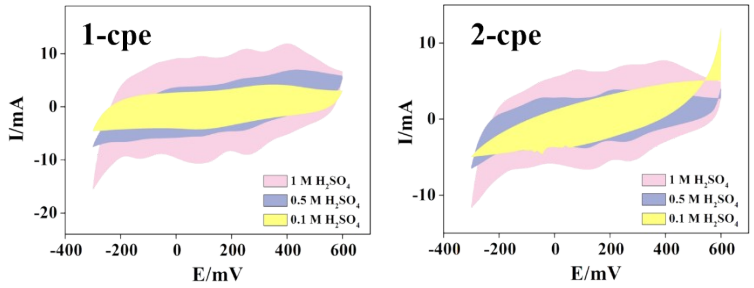

Fig. S5. The CV curves of **1**-cpe and **2**-cpe in different electrolyte.

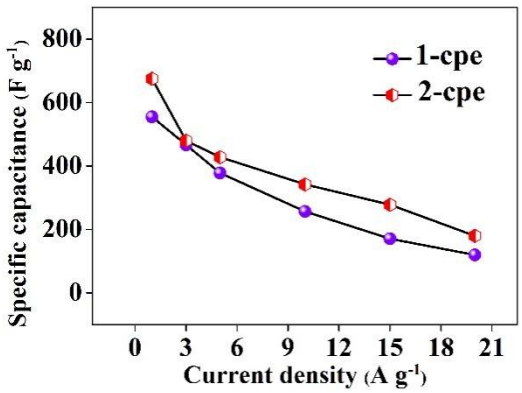

Fig. S6. The specific capacitance of **1**−**2**-cpes at different current densities.

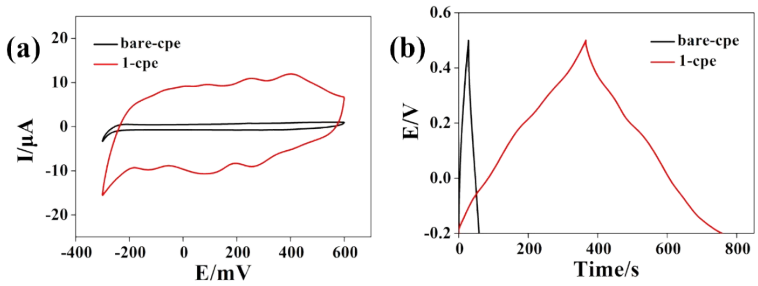

Fig. S7. (a) The CV curves of bare-cpe and **1**-cpe when the scan rates were 10 mV s^{-1}; (b) the GCD curves of bare-cpe and **1**-cpe at a current density of 1 A g^{-1}.

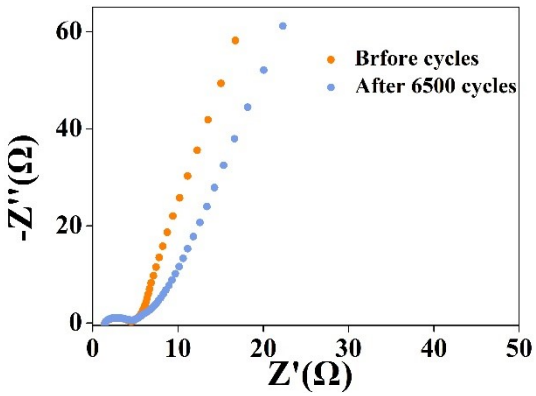

Fig. S8. The EIS of symmetrical supercapacitor device before and after cycles.

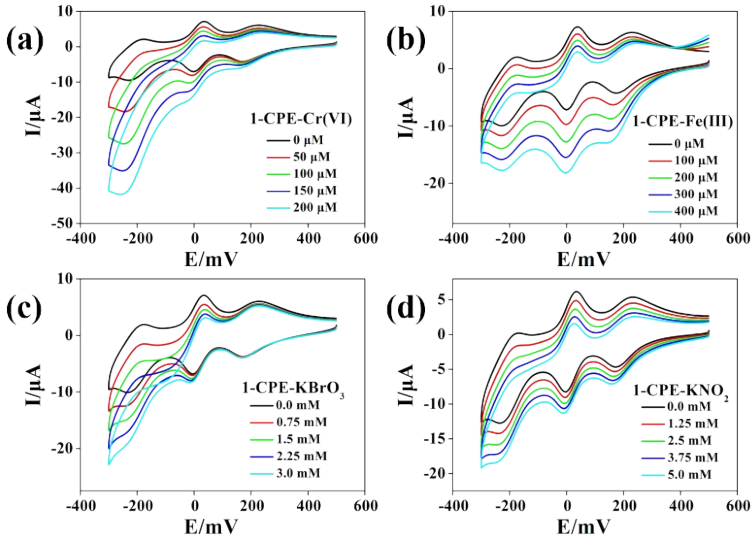

Fig. S9. The CV curves of **1**-CPE with the addition of different concentrations of (a) Cr(VI); (b) Fe(III); (c) $KBrO_3$; (d) KNO_2.

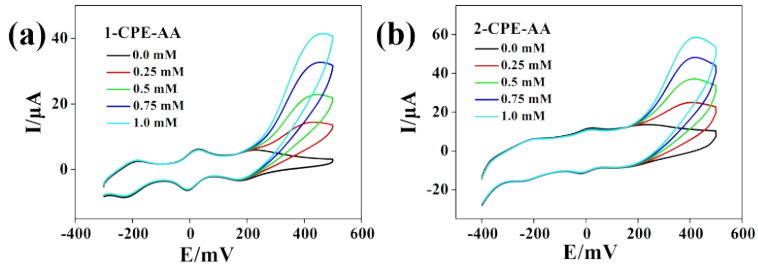

Fig. S10. (a-b) The CV curves of **1**–**2**-CPEs with the addition of different concentrations of AA.

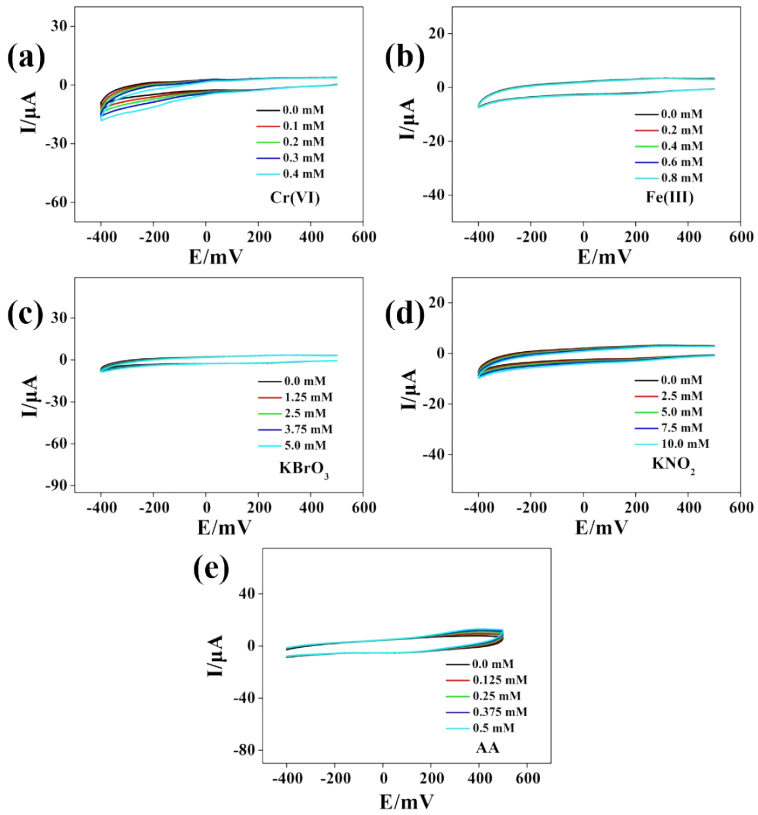

Fig. S11. The CV curves of bare-CPE with the addition of different concentrations of (a) Cr(VI); (b) Fe(III); (c) $KBrO_3$; (d) KNO_2 and (e) AA.

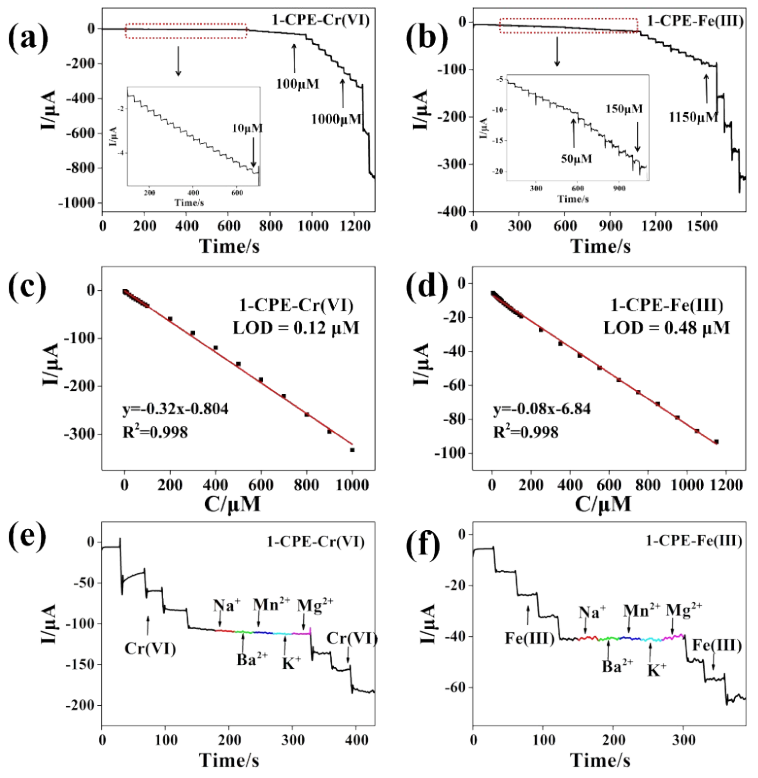

Fig. S12. The I-t curves of **1**-CPE for (a) Cr(VI) and (b) Fe(III); The linear relationship of **1**-CPE for (c) Cr(VI) and (d) Fe(III); The interference immunity performances of **1**-CPE for (e) Cr(VI)

and (f) Fe(III).

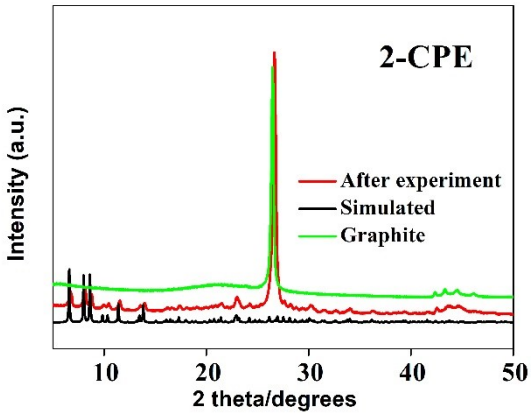

Fig. S13. The PXRD pattern of **2**-CPE after the sensing experiments.

Table. S3 The comparison table of specific capacitance (Cs) for reported POM-based crystal materials electrode.

Electrode	C_s ($F\ g^{-1}$)	Current density ($A\ g^{-1}$)	Ref.
1-cpe	555	1	This work
2-cpe	675	1	This work
$[Cu^{I}_4H_2(btx)_5(PMo_{12}O_{40})_2]\cdot 2H_2O$	237	2	6
$[Cu^{II}Cu^{I}_3(btx)_5(SiMo^{VI}_{11}Mo^{V}O_{40})]\cdot 4H_2O$	138	2	6
$[Cu^{I}H_2(C_{12}H_{12}N_6)(PMo_{12}O_{40})]\cdot[(C_6H_{15}N)(H_2O)_2]$	249.3	3	7
$[Cu^{II}_2(C_{12}H_{12}N_6)_4(PMo^{VI}_9Mo^{V}_3O_{39})]$	154.5	3	7
$(Hbipy)_3[PMo_{12}O_{40}]\cdot 3H_2O$	263.9	1	8
$H\{Zn_4(DIBA)_4[(DIBA)(HPO_2)]_2(\alpha\text{–}PMo^{I}_8Mo^{V}_4O_{40}Zn_2)\}$	171.17	0.5	9
$[\varepsilon\text{–}PMo^{V}_8Mo^{VI}_4O_{37}(OH)_3Zn_4(HDBIBA)_2]\cdot 6H_2O$	146.77	0.5	9
$([Zn_4(BTC)_2(\mu_4\text{-}O)(H_2O)_2]@Ag_5[BW_{12}O_{40}]$	161.7	1	10
$H_3PMo^{VI}_{12}O_{40}\cdot(BPE)_{2.5}\cdot 3H_2O$	137.5	2	11

Table. S4 Comparison of **1**−**2** with other reported POM-based crystal sensors for the determination of Cr(VI).

Materials	Method	Sensitivity ($\mu A\ \mu M^{-1}$)	LOD (μM)	Ref.
1-CPE	I-t	0.32	0.12	This
2-CPE	I-t	0.40	0.10	This
$[Cu^{II}_4(btmc)(ctcm)_4(\beta\text{-}Mo_8O_{26})]\cdot[\beta\text{-}Mo_8O_{26}]\cdot H_2O$	I-t	0.015	0.074	12
$[Cu^{II}_4(mct)_2(ctcm)_2(H_2O)_6(\beta\text{-}Mo_8O_{26})]\cdot[\beta\text{-}Mo_8O_{26}]$	I-t	0.08	0.25	12
$[Cu_2(bpae)_2(\beta\text{-}Mo_8O_{26})]\cdot 6H_2O$	I-t	0.02	0.51	13
$(H_2bpp)_6\{GdMo^{V}_2Mo^{VI}_{16}O_{49}(HPO_4)_3(PO_4)_3\}_2\cdot 11H_2O$	I-t	0.151	0.202	14
$(H_2bpp)_2[Na_4Fe(H_2O)_7][Fe(P_4Mo_6O_{31}H_6)_2]\cdot 2H_2O$	I-t	0.117	0.174	15
$(H_2bpp)_6(bpp)_2[Fe(P_4Mo_6O_{31}H_8)_2]_2\cdot 13H_2O$	I-t	0.074	0.33	15

Table S5 Parameters for Cr(VI) and Fe(III) determination using **1**–**2**-CPEs.

		Detection limit ($\mu mol\ L^{-1}$)	**Sensitivity ($\mu A\ \mu M^{-1}$)**	**Linear Range ($\mu mol\ L^{-1}$)**
1-CPE	Cr(VI)	0.12	0.32	0.5-1000
	Fe(III)	0.48	0.08	5-1150
2-CPE	Cr(VI)	0.10	0.40	0.5-1000
	Fe(III)	0.38	0.11	5-1150

References

1. O. V. Dolomanov, L. J. Bourhis, R. J. Gildea, J. a. K. Howard, H. Puschmann, *J Appl Crystallogr*, 2009, **42**, 339.

2. T. Zhao, L. P. Cui, K. Yu, J. H. Lv, Y. J. Ma, A. S. Yang, B. B. Zhou, *ACS Appl Mater Interfaces*, 2022, **14**, 30099.

3. Y. Hou, D. F. Chai, B. N. Li, H. J. Pang, H. Y. Ma, X. M. Wang, L. C. Tan, *ACS Appl. Mater. Interfaces*, 2019, **11**, 20845-20853.

4. Y. Tian, Z. H. Chang, X. L. Wang, H. Y. Lin, Y. C. Zhang, Q. Q. Liu, Y. Z. Chen, *Chem. Eng. J*, 2022, **428**. 132380.

5. R. J. Liu, Y. Y. Luo, Y. H. Zheng, G. J. Zhang, C. Streb, *Chem Commun*, 2020, **56**, 9465-9468.

6. D. Chai, C. J. Gómez-García, B. Li, H. Pang, H. Ma, X. Wang, L. Tan, *Chem. Eng. J.*, 2019, **373**, 587-597.

7. D. F. Chai, J. J. Xin, B. N. Li, H. J. Pang, H. Y. Ma, K. Q. Li, B. X. Xiao, X. M. Wang, L. C. Tan, *Dalton Trans*, 2019, **48**, 13026-13033.

8. L. Y. Zhang, X. Y. Zhao, C. M. Wang, K. Yu, J. H. Lv, C. X. Wang, B. B. Zhou, *J Solid State Chem.*, 2022, **312**, 123235.

9. X. Wang, H. Li, J. F. Lin, C. Y. Wang, X. L. Wang, *Inorg Chem*, 2021, **60**, 19287-19296.

10. L. Y. Wang, N. Kang, L. G. Gong, C. X. Wang, K. Yu, C. M. Wang, B. B. Zhou, *J Energy Storage*, 2022, **46**, 103873.

11. C. L. Wang, S. Rong, Y. Q. Zhao, X. M. Wang, H. Y. Ma, *Transit. Metal Chem.*, 2021, **46**, 335.

12. C. Wang, J. Ying, H. C. Mou, A. X. Tian, X. L. Wang, *Inorg Chem Front*, 2020, **7**, 3882.

13. X. L. Wang, Z. W. Cui, H. Y. Lin, Z. H. Chang, *CrystEngComm*, 2021, **23**, 2113.

14. J. Q. Niu, Y. Y. Ma, X. Xin, Z. G. Han, *Cryst. Growth Des*, 2020, **20**, 3584-3589.

15. X. Xin, N. Hu, Y. Ma, Y. Wang, L. Hou, H. Zhang, Z. Han, *Dalton Trans*, 2020, **49**, 4570.